Computers in Biology and Medicine 58 (2015) 118–129

Contents lists available at ScienceDirect

Computers in Biology and Medicine

journal homepage: www.elsevier.com/locate/cbm

Modeling and simulation of a low-grade urinary bladder carcinoma

Svetlana Bunimovich-Mendrazitsky [a], Vladimir Pisarev [b,c,d], Eugene Kashdan [e,*]

[a] Department of Computer Science and Mathematics, Ariel University, Ariel 40700, Israel
[b] V.A. Negovsky Research Institute for General Reanimatology, 25 Petrovka, Bldg. 2, Moscow 107035, Russian Federation
[c] D. Rogachev Federal Clinical Research Center for Children Hematology, Oncology and Immunology, 1 Samory Mashela St., Moscow 117198, Russian Federation
[d] University of Nebraska Medical Center, Omaha, NE 68198, USA
[e] School of Mathematical Sciences, University College Dublin, Belfield, Dublin 4, Ireland

ARTICLE INFO

Article history:
Received 11 October 2013
Accepted 26 December 2014

Keywords:
Bladder cancer
Angiogenesis
Cellular automata
Nonlinear diffusion-absorption equation
Hybrid model

ABSTRACT

In this work, we present a mathematical model of the initiation and progression of a low-grade urinary bladder carcinoma. We simulate the crucial processes affecting tumor growth, such as oxygen diffusion, carcinogen penetration, and angiogenesis, within the framework of the urothelial cell dynamics. The cell dynamics are modeled using the discrete technique of cellular automata, while the continuous processes of carcinogen penetration and oxygen diffusion are described by nonlinear diffusion–absorption equations. As the availability of oxygen is necessary for tumor progression, processes of oxygen transport to the tumor growth site seem most important. Our model yields a theoretical insight into the main stages of development and growth of urinary bladder carcinoma with emphasis on the two most common types: bladder polyps and carcinoma *in situ*. Analysis of histological structure of bladder tumor is important to avoid misdiagnosis and wrong treatment. We expect our model to be a valuable tool in the study of bladder cancer progression due to the exposure to carcinogens and the oxygen dependent expression of genes promoting tumor growth. Our numerical simulations have good qualitative agreement with *in vivo* results reported in the corresponding medical literature.

1. Introduction

Bladder cancer (BC) represents an increasing health problem worldwide. It is estimated that around 400,000 new cases are diagnosed annually and 150,000 people die directly from BC each year. The highest incidence of BC occurs in the industrialized and developed countries in Europe, North America, and Northern Africa. According to the current statistics urinary bladder carcinoma is the fourth most common new cancer in men and ninth in women [1].

A number of risk factors have been strongly linked to the development of BC. Roughly 20% of all BC cases have been related to occupational exposure to chemicals and dye, mostly in industrial areas processing paint, metal, and petroleum products. Tobacco smoking is the main BC risk factor, accounting for at least 30% of BC cases. Epidemiological and experimental evidence has also implicated environmental carcinogens in the aetiology of BC. Exposure to arsenic in drinking water has been recognized as a cause of BC, for instance, in a study of long-term impact of arsenic pollution observed in Chile. BC mortality was significantly higher in affected regions more than 20 years after cessation of pollution [2].

The first model of carcinogen penetration and BC initialization was proposed by Kashdan and Bunimovich-Mendrazitsky [3]. It was based on the evidence of BC origins and the biological properties of the urothelium and included a porous medium type equation to model carcinogen penetration combined with the cellular automata (CA) simulation of cell dynamics. In [3], the authors assumed that the tissue was well oxygenated and the angiogenesis had not started. Thus it was aimed to simulate the BC initiation and the first steps of the superficial polyp growth. However, it laid a basis of the high fidelity model presented in this paper that reproduces the state and behavior of multiple mechanisms involved in BC development. In this work, we introduce continuous oxygen and nutrient diffusion, and address hypoxia as one of the regulating factors in the cell cycle for both normal and cancerous cells. In order to simulate tumor growth beyond its initial stages we embed in the model a mechanism responsible for the development of the neovascular network providing tumor cells with additional oxygen and nutrients necessary for their continuous proliferation (a process known as *angiogenesis*).

Our research is based on the hypothesis that BC development is a multiscale multilevel process. The “building blocks” of our model

* Corresponding author.
E-mail addresses: svetlanabu@ariel.ac.il (S. Bunimovich-Mendrazitsky), vpisarev@gmail.com (V. Pisarev), ekashdan@maths.ucd.ie (E. Kashdan).

http://dx.doi.org/10.1016/j.compbiomed.2014.12.022
0010-4825/

are: (i) carcinogen penetration into the urothelium and (ii) oxygen diffusion, influenced by (iii) angiogenesis. Our approach to BC modeling corresponds with the multiscale studies of brain gliomas [4] and colorectal cancer [5] that eventually led to novel therapeutic strategies to treat these diseases.

The first goal of this work is to analyze various tumor development scenarios leading to angiogenesis. The second goal is to provide a basis for BC therapy personalization through the simulation of BC progression under various conditions. In the numerical experiments presented in this paper, we discuss a number of scenarios involving low-grade urothelial carcinomas such as superficial bladder polyp and carcinoma *in situ* (CIS). However, our model is not limited to these cases and it could simulate the invasive form of BC in conjunction with the model of tumor invasion.

The mathematical model of invasive BC is based on the interaction (and the competition) between the matrix metalloproteinases (MMP), produced by the cancerous cells, and the tissue inhibitors of metalloproteinases (TIMP), secreted by the tissue to confront the tumor progression, was introduced and studied in [6]. The paper is organized as follows: In Section 2, we present general information about the BC and the biological background of our model. After which we provide the reader with the model framework, divided into three consecutive sections: (a) The CA model of the urothelial cell dynamics (Section 3). (b) Continuous processes, which correspond to oxygen diffusion and carcinogen penetration (Section 4). (c) Modeling angiogenesis (Section 5). Section 6 is dedicated to numerical simulations and a discussion of a number of scenarios leading to tumor development and progression. We conclude our paper in Section 7.

2. Biological background

2.1. Normal urothelium

A human bladder consists of the following layers: bladder lumen, urothelium, lamina propria, muscle and fat [7,8] as sketched in Fig. 1.

The urothelium is a highly specialized layer of epithelial cells lining the bladder. It has to maintain a tight barrier against urea and other toxins, while accommodating large changes in bladder volume. The epithelial cells of the urothelium form part of an integrated network, which plays a major role in bladder sensory system. It is responsible for local circulation of blood and removal of pathogens. Under normal conditions the urothelium has a very low cell turnover rate. However, when the urothelium is damaged it has to repair itself rapidly [7,9]. The balance between the cell proliferation and differentiation controls the cell replacement process.

The urothelium is composed of three to six layers of cells including basal cells, intermediate cells and superficial (umbrella)

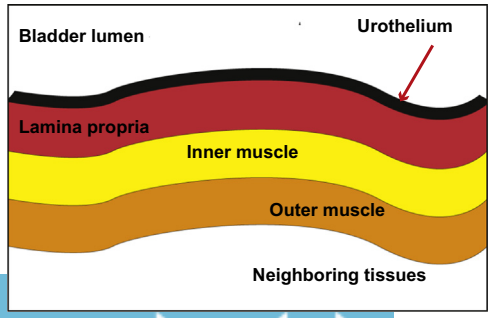

Fig. 1. The structure of human bladder.

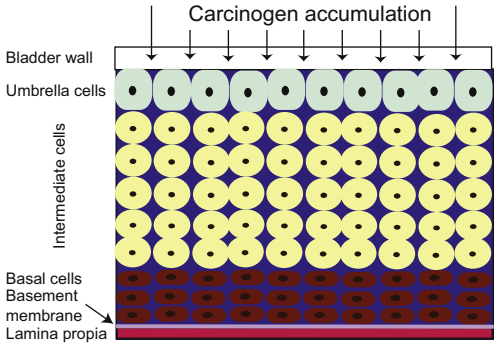

Fig. 2. The structure of the urothelium. (Reproduced with publisher permission [3].)

cells (Fig. 2). Basal cells are germinal in nature and approximately 5–10 μm in diameter. The basal cells are the only cells in a normal urothelium that could proliferate and move between layers after differentiation (if needed). The basal cells replace dead intermediate and umbrella cells by accepting the phenotype corresponding to each layer [7]. The cell replacement process is discussed in more detail in Section 3. The layer containing basal cells includes rare normal stem cells, which have a potential to initiate tumor growth [10,11]. It has been well established that tumor-initiating cells (stem cells or stem-like cells), originating from normal stem cells or from cells, which have transformed back from differentiated cells due to mutations, are responsible for initiation, control and metastatic spread of numerous tumors including urothelial cancer (see review in [11]). Accumulation of carcinogenic mutations in normal stem cells due to continuous action of environmental carcinogenic compounds is crucial to initiate and drive the carcinogenesis due to the altered expression of genes, affecting key signaling pathways of the cell. Most recent studies have demonstrated that abnormal overexpression, even of one protein in stem cells, within the basal urothelium in mice might generate an invasive lesion resembling all patterns of human bladder carcinoma *in situ* [12].

Intermediate cells are superficial to the basal cells and larger than them (about 20 μm in diameter). The luminal surface of the urothelium is formed by the umbrella cells (the largest epithelial cells in the body, between 100 μm and 200 μm in diameter [8]). The bladder urothelium shrinks (20–50%) during the urination process. When the bladder fills the number of cell layers reduces as the cells flatten to accommodate the stretching of the bladder wall [13].

As with any epithelial tissue, the normal (healthy) urothelium obtains oxygen and nutrients through diffusion from the capillary network located in the lamina propria and is separated from the urothelium by the basement membrane [3,7].

2.2. BC classification and grading

The most recent 2004 WHO classification distinguishes four grades of urothelial tumors in accordance with their malignancy (from low to high) [7]:

1. Urothelial papilloma.
2. Urothelial neoplasm of low malignant potential.
3. Papillary urothelial carcinoma, low-grade.
4. Papillary urothelial carcinoma, high-grade.

In this work, we model the low-grade papillary urothelial carcinoma. However, our approach is not limited to this type of

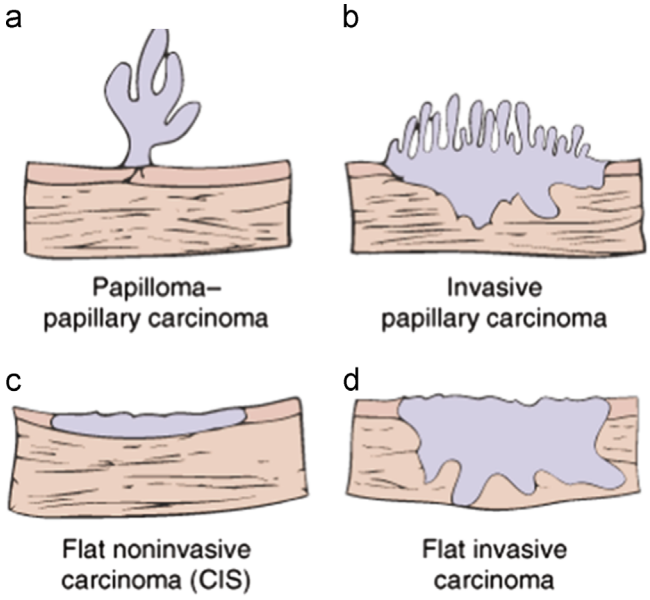

Fig. 3. Patterns of urinary bladder carcinoma. (Reproduced with publisher permission [7].)

BC and the model could be generalized to the simulation of high-grade carcinoma as well.

There are four morphological patterns of bladder tumors as shown in Fig. 3. Our particular interest belongs to the non-invasive papillary carcinoma (also known as *polyp* or *papilloma*) and the flat non-invasive carcinoma (carcinoma *in situ* – CIS) responsible together for approximately 75% of diagnosed BC cases [14]. As sketched in Fig. 3(a), the noninvasive papillary carcinoma passes through the bladder wall into the bladder lumen but goes no deeper than the lamina propria. On the other hand, CIS (Fig. 3(c)) remains within the urothelium. If not treated properly, both polyp and CIS could transform into the far more dangerous invasive forms. In Fig. 3, this corresponds to the (a)→(b) and (c)→(d) transformations. It is estimated that between 15% and 30% of low-grade carcinomas will progress to the high-grade [14]. Statistically, CIS has more chances to progress to the high-grade (invasive) urinary bladder carcinoma than the polyp [15].

2.3. Tumor dynamics and carcinogenesis pathways

The main factor responsible for BC initiation is an accumulation of genetic alterations (DNA mutations) in stem-like cells within the bladder urothelium, capable of triggering abnormal signaling through key molecular networks. Similar to other malignancies, it is likely that bladder carcinogenesis involves aberrations in cell differentiation and proliferation, often with the derangement in the genetic composition of malignant cells. Conversion of normal urothelial cells to cancer cells and progression from the low-grade to the high-grade muscle-invasive cancer are the result of the sequential acquisition of somatic gene mutations [16]. We refer the reader to Table 1 in [17] for the list of the gene alterations common in bladder cancer and to the scheme of molecular and genetic pathways for bladder tumor classification in [18].

Different carcinogens act on cells in different ways. However, they all have certain aspects in common. There are two ways the carcinogens use to damage genetic composition of cells: by direct DNA modifications or through inducing gross chromosomal abnormalities. The first interaction of the cell with carcinogen does not lead to the cancerous mutations (e.g., loosing its growth control). Affected cell must undergo at least one cell division to move from pre-cancerous to cancerous state. Only following DNA and chromosome replication, the cell starts to acquire the cancerous behavior pattern [19].

In case of BC, there are two pathways of carcinogen activation [20]. For several compounds with carcinogenic or co-carcinogenic activities their accumulation could be critical for dose-dependent, sequential accumulation of mutations in tumor-initiating cells. Metal ions, proved to be accumulated in human tissues and to induce tumors *in vitro* or *in vivo*, are prime candidates for such effects [21]. Prolonged exposure to heavy metals including arsenic and cadmium were found to enhance mutagenicity and carcinogenicity, or, even directly to induce malignant transformation of non-malignant immortalized cells [21–23]. Evidence is growing that prolonged exposure to heavy metals of gene expression profiles of epithelial cells is consistent with the malignant phenotype of cells [24–26]. The metal traces quantification in bladder biopsies from tumoral, non-cancerous areas, adjacent to tumors, and normal tissues, revealed significantly elevated levels of two carcinogens, arsenic and cadmium, in adjacent to tumor areas [27]. The accumulation of metals and possibly other carcinogenic compounds in the microenvironment might increase the likelihood of genetic instability and multiple mutations of tumor-initiating cells located within the field of cancerization.

Another pathway is exposure to chemical carcinogens, for instance, aromatic amines, associated with smoking [20]. These carcinogens are excreted in the urine and stored temporarily in the bladder. They interact with the urothelium through penetration. The chromosomal damage is gradually accumulating in the urothelial cells and eventually leads to the change in their phenotypic expression and transformation into overt neoplasm.

One should note that increased carcinogen concentration could yield non-cancerous gene alterations as well. However, in this paper we consider the mutation sequence that leads to the malignancy only. In fact, invasive and non-invasive forms of BC correspond to the different sequences of the DNA mutations [18,28]. According to [28] it takes between three to five mutations for a cell to obtain a cancerous phenotype that corresponds to the superficial polyp or carcinoma *in situ*. This result agrees with [17,18], where four mutations are considered necessary to initiate development of bladder cancer.

As highlighted above, BC is a complex phenomenon, which involves the number of physical and biological processes. The main features responsible for BC development and progression are the alteration of tumor-initiating cell DNA due to the carcinogen penetration from the bladder and angiogenesis [16]. Both these processes crucial for tumor development and growth are modeled in our work. In our computational experiments, we investigate the possible role of insufficient oxygen supply (hypoxia inducible factor – HIF) in the progression of the low-grade urinary bladder carcinoma, and examine its expression in relation to the cell turnover and the proliferation status.

3. Computational model of urothelial cell dynamics

We have chosen the cellular automata (CA) formulation for representation of cell dynamics in the urothelium. CA allows us to model intuitively the critical parameters governing tissue regulatory mechanisms: cell proliferation, apoptosis (cell death), and dynamics of both normal and cancer cells [29]. All these mechanisms include a number of sub-processes (i.e. maturation) that have also been taken into account. The lattice for our model is formed by the slice of the bladder tissue as shown in Fig. 4(a). Our basic unit is one urothelial cell. Bladder size estimations vary in the literature. The anatomy and physiology textbook [8] reports average volume of bladder as 600 mL. The approximate size of the urothelium cross-section that we are looking on is

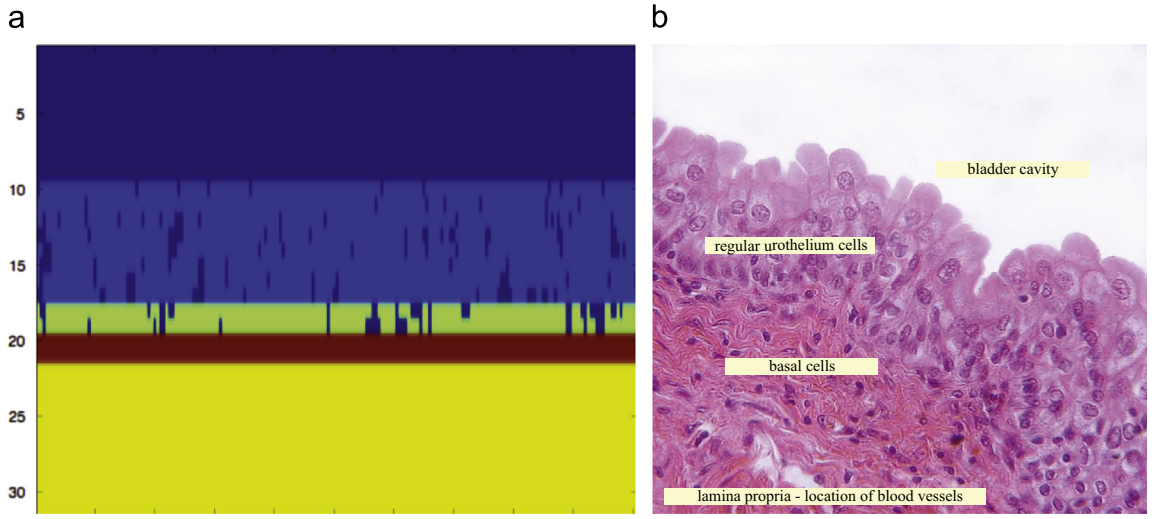

Fig. 4. Modeled slice of normal urothelium (a) and actual image of the fragment of the urothelium obtained from cystoscopy [30] (b). The colors on the left plot, from top to bottom, are as follows: dark blue – the bladder lumen and the empty space inside the urothelium; light blue – ordinary (umbrella and intermediate) urothelial cells; green – the basal cells; red – blood vessels; yellow – muscle and fat layers. (Reproduced with publisher permission [6].) (For interpretation of the references to color in this figure caption, the reader is referred to the web version of this paper.)

330 mm × 0.2 mm. In the numerical simulations we consider a 4 mm × 0.2 mm fragment of the urothelium cross-section.

In accordance with [29] our CA model is formed as a two-dimensional array of automaton elements. Each element corresponds to the urothelial cell as shown in Fig. 4(b). The cell characteristics change along the vertical axis representing the layers of the urothelium. In our previous publications [3,6], we defined the following morphological structure as a basis for our CA algorithm:

- The top 9 rows represent the bladder lumen.
- The next 10 rows of the lattice (10–19) constitute the urothelium. Superficial polyps start within the urothelium, break the bladder wall and grow within the lumen.
- The blood vessels located in lamina propria occupy rows 20 and 21.
- Below lamina propria we place fat and muscle layers to model the invasive forms of BC.

The state vector represents cell dynamics of each CA cell. In the model implemented in this work, the state vector has six components: (i) the site of the cells: lumen, umbrella and intermediate layers (that we address as *ordinary urothelial cells*), basal layer, lamina propria (where blood vessels reside), fat and muscle layer; (ii) occupation status, i.e. whether the element is occupied by the normal cell, the mutated cell, by the "empty space" or by the blood vessel; (iii) the cell status, i.e. whether the basal cell is in the proliferative or in the interphase state; (iv) the carcinogen concentration; (v) cancerous mutation counter of the cell; and (vi) oxygen and nutrients level.

The state vector evolves in time according to the prescribed local rules, used to update any given element from its own state and that of its neighbors on the previous time step. The structure called "urothelium state" characterizes every cell and it is filled during the numerical simulation. The CA model presented in this paper is the enhanced and expanded version of the CA approach proposed in [3,6]. The general flowchart of the algorithm is shown in Fig. 5 and the flowcharts describing the CA rules corresponding to the different types of cells are presented in Figs. 6–7.

Our model represents differences in the behavior of normal (basal and ordinary) and cancer cells as follows:

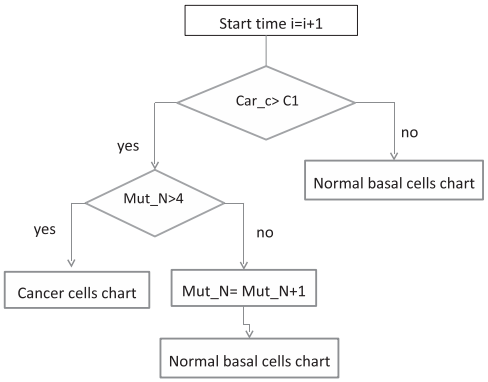

Fig. 5. The CA rules corresponding to the state vector evolution. *Car_c* and *Mut_N* represent the carcinogen concentration level and the mutation counter respectively; *C1* is the carcinogen threshold from Table 1.

- *Normal basal cells containing tumor-initiating cells*: The stem cells of the urothelium are located within the basal layer. The hypothesis that the basal cells are routinely lost and replaced had been experimentally confirmed. The stem cells form a balanced (proliferation vs. differentiation) population due to the frequent cell loss and replacement [31]. The cell division depends on the dynamics of clonal population and anatomic constraints [32].
  Stem cells (including tumor-initiating cells) are self-renewing cells that can divide asymmetrically to yield a new stem cell and a progenitor cell [10]. Progenitor cells, in their turn, might (but not must) undergo further divisions. However, eventually they will stop dividing and leave the cell cycle through terminal differentiation. Most tissues in the human body are made up of such non-dividing cells. In a healthy tissue, the process of cell proliferation is always under strict control and it is limited to the needs of tissue growth and renewal. However, multiple mutations accumulating in somatic cells in a years-long span destroy the control mechanism that would otherwise prevent cancer cells division. Uncontrolled cell proliferation is one of the hallmarks of cancer.
  The following CA rules (see also flowchart in Fig. 6) are applied to each basal cell as the algorithm progresses from the time-step i to the time-step $i+1$:

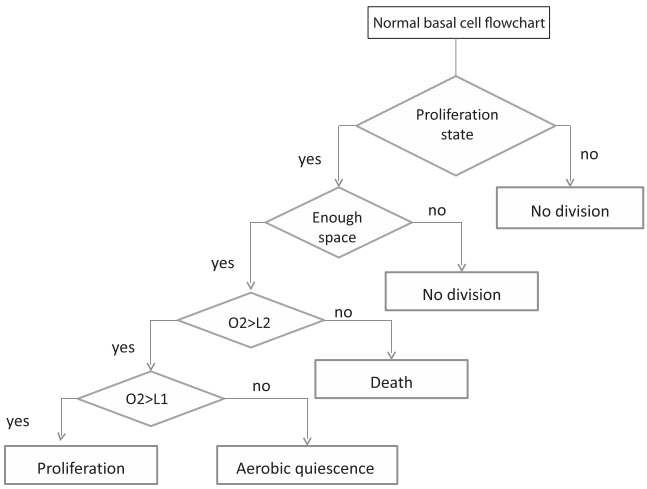

Fig. 6. The CA rules corresponding to the basal cell proliferation rules. *O2* is the oxygen concentration. *L*1 and *L*2 correspond to the oxygen thresholds for normal cells, given in Table 1. *L*1 is the proliferation threshold and *L*2 is the apoptosis under hypoxia threshold.

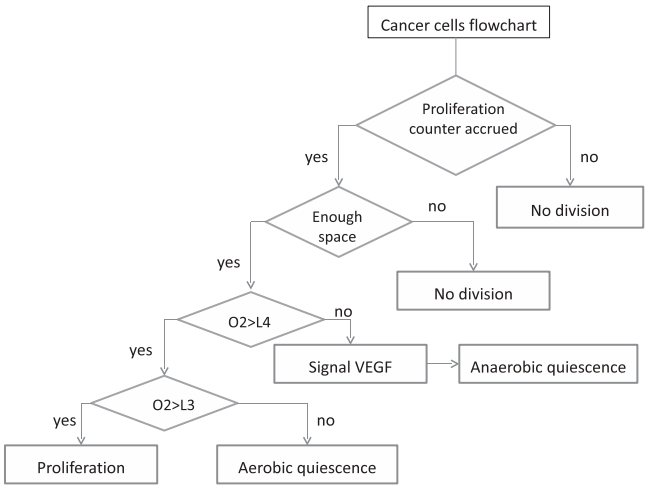

Fig. 7. The CA rules corresponding to the cancer cell proliferation rules. *O2* is the oxygen concentration level. *L*3 and *L*4 correspond to the oxygen thresholds for cancer cells, given in Table 1. *L*3 is the proliferation threshold and *L*4 is the dormancy state threshold.

1. Cell death in urothelium (either necrosis or apoptosis) initiates the signal for proliferation and provides nutritional support that reaches the basal level containing stem cells. The experiments confirm that the injured or dying cells might produce or liberate molecules signaling to the rare subsets of stem or progenitor cells from the basal layer [33]. Provided that the signal for empty place exists, and the cell is ready to proliferate, we turn the proliferation flag *on* for the next iteration. The cell has multiple mechanisms to control its nutritional status and oxygen concentration. If oxygen and nutrients are insufficient, the cell will not divide [34].
2. If more than one cell is ready for proliferation then the closest cell to the empty space will be chosen; if more than one cell could fill the empty space then the choice is made by "throwing the dice". The process is detailed as follows:
   - If the oxygen level at the element occupied by the cell is above the threshold *L*1, then we sample the region around the element in order to determine whether the cell division occurs or not.
   - If the cell is in the proliferative state, it will divide to form two daughter cells, of which one will replace (renew) it, and another will move into the "empty" site.
   - If the cell does not get the signal it will attempt to divide on the next iteration.
3. Every basal cell accumulates carcinogen; if carcinogen concentration passes the threshold *C*1 we add one to the cancerous mutation counter; as soon as the BC mutation counter is equal to four, the cell obtains cancer phenotype and behaves according to the cancer cell mode described below. Carcinogens yield various DNA mutations, many of which are not cancerous. However, the mutation process is not entirely random. In [35], the authors traced the mutational evolution of individual tumors and reconstructed the order of occurrence of abnormalities in individual tumors based in the DNA sequence and copy number information. In particular, they succeeded to follow the evolution of individual tumors into two separate cancers. Our assumption is that the concentration of carcinogen above the threshold leads to the first of the mutations in the BC sequence and consequently to the rest of mutations down the road. As confirmed by the experiments, the time-line of the mutations accumulation process could vary from few days as result of a massive urothelial cell loss due to the bladder injury or inflammation, to a number of years in case of the regular turnover of the urothelial cells.
4. The daughter cells inherit the mutation counter and the carcinogen concentration from their mother cell. There is no information, regarding proportion of carcinogen inheritance between the daughter cells. However, as a result of the chronic exposure to the carcinogens coming from outside this value is not important. Due to the diffusive properties of the continuous model of carcinogen penetration discussed in Section 4.2, the carcinogen concentration in every single cell is similar to the concentration in its neighbors and the outliers are fixed within a few very short time-steps of the continuous model. In fact, the carcinogen penetration increases the probability of malignization, but does not force it. The major reason behind BC is the accumulation of genetic damage under effect of carcinogens that leads to the mutations. In some cases, the DNA could be repaired and the cells could either survive or die in this process. However, when the mutations necessary for carcinogenesis build up, and there exists a micro-environment (e.g., an inflammation leading to the massive cell death), the tumor starts to grow.
5. The basal cell has two oxygen concentration thresholds: *L*1 (enough for proliferation) and *L*2 (sufficient for life, but insufficient for proliferation); the oxygen level below *L*2 leads to the cell death from the hypoxia.
6. In order to differentiate, the basal cell should satisfy the following conditions:
   (a) The cell should be in the proliferative state.
   (b) The cell should have sufficient oxygen concentration (above *L*1).
   (c) The cell proliferation flag is turned *on* (as result of the appropriate signal from the ordinary cell as described below).

The average length of the cell cycle is 1 day, which corresponds to one iteration in the CA algorithm.

- *Ordinary (umbrella and intermediate) cells:* In process of cell turnover, older differentiated cells are typically eliminated by apoptosis and replaced by the division progeny of stem cells [36]. In fact, the urothelium has one of the lowest turnover rates among mammalian epithelia, estimated as once a year [37]. We set the threshold of the oxygen concentration for the

ordinary cell equal to $L2$ (same as for the basal cell). The CA rules are applied to the ordinary cells as follows:

1. The dying cell sends a signal to the basal (stem) cells that the empty space has emerged and could be filled.
2. The ordinary cell could die in three cases:
   (a) *apoptosis* – natural death after 12 months [37];
   (b) *apoptosis under hypoxia* – death due to the lack of oxygen (the oxygen level is below $L2$) [38];
   (c) *necrosis* – when the carcinogen concentration is above the threshold $C1$ [39].

- *Cancer cells*: At each time step, the CA algorithm checks the carcinogen concentration for every cell. If the concentration passes the threshold level the first mutation is registered in accordance with [40]. Different carcinogens have different mutation threshold values. Therefore simultaneous exposure to multiple carcinogens could significantly accelerate mutations rate. The DNA mutations caused by carcinogens may occur in any cell of the urothelium. However, in ordinary cells they yield the cell death. Only stem cells located in the basal layer can transfer their genetic alterations to the daughter cells, which in their turn might eventually become cancerous following the number of cell divisions [39]. Thus we examine mutations on the basal layer only.
  The cancer cell behaves according to the following set of rules (Fig. 7):
  1. The cancer cells can differentiate anywhere in urothelium and they compete with the normal cells for empty space.
  2. A tumor cell could survive with concentration of carcinogen above $C1$.
  3. Cancer cells have their own oxygen thresholds: if the oxygen level in the cancer cell is less than $L3$ it produces a signal, which is sent to the vascular system in order to start sprouting of blood cells towards the area with the lack of oxygen (angiogenesis). In this case, the cancer cell cannot proliferate.
  4. If the oxygen concentration is below $L4$ the cancer cell enters the hypoxia-induced dormancy state for one year and only after that, if the oxygen supply does not increase above the threshold, the cancer cell dies.
     This rule corresponds to a well known, but not exclusive, feature of cancer cells – their ability to enter a quiescent state under hypoxic conditions, in which they suspend all activity, including any cell division that is not essential for survival [41]. The duration of the hypoxia-induced dormancy state varies between approximately 2 months and 1 year depending on the cancer. There is also difference between *in vivo* and *in vitro* experiments [42]. However, we have found numerically that varying this parameter between 9 months and 1 year (an estimated range for tumor-initiating epithelial cells) has very little impact on tumor progression due to renewed oxygen supply via the angiogenic network of blood vessels.
- *Interaction between the models*: At each time step the CA model interacts with the continuous models of carcinogen penetration and oxygen diffusion by supplying them with the state vector information and obtaining the levels of carcinogen and oxygen concentration correspondingly as shown in Fig. 8.

4. Continuous processes

4.1. Oxygen diffusion

In Section 2.1, we pointed out that one of the major characteristics of the normal urothelium (and any other transitional epithelium) is an absence of the blood vessels. The oxygen and nutrients reach the urothelial cells through passive diffusion. The oxygen diffusion model allows us to investigate the possible role of Hypoxia Inducible Factor (HIF) in the recurrence and the progression of low-grade urinary bladder carcinoma, and to examine its expression in relation to cell proliferation, apoptosis and angiogenesis [43].

We describe the process of oxygen diffusion using the nonlinear diffusion-reaction equation, based on the porous medium equation with the absorption term:

$$\begin{cases} \partial_t u - \nabla[D(\vec{x},t)\nabla(|u|^{m-1}u)] + h(t)|u|^{q-1}u = f(\vec{x},t) \quad \text{in } Q_N^T, \\ u(\vec{x},0) = k\delta_0. \end{cases} \tag{1}$$

We call $u(\vec{x},t)$ the concentration of oxygen measured in [amount of oxygen per cell volume]=[mol/L]. The diffusion coefficient $mD(\vec{x},t)|u|^{m-1} > 0$ has dimensions of [cell area on lattice per unit of time]=[cm^2/s] and it is proportional to the degree $m-1$ of u, where $m > 1$. When $m=1$, we have linear diffusion, which has infinitely fast speed (impossible from the biological point of view). While D is usually known or can be measured, the value of m is adjusted using numerical experiments. Cells can absorb water, oxygen or even salt through passive transport. The plasma membrane allows relatively small molecules to enter and exit the cell, but does not allow larger molecules to pass. To simulate this process we add non-differentiated absorption term $qh(t)|u|^{q-1} > 0$, the units of which are [s^{-1}]. The rate of absorption is proportional to the degree $q-1$ of concentration ($q > 1$), which is also adjusted in numerical experiments. Initially oxygen concentration is random within the urothelium and is maximal in the blood vessels within lamina propria. This situation is represented by the initial condition and the source term $f(x,t)$. The changes in oxygen diffusion that correspond to angiogenesis are discussed in Section 5.

Our domain of interest Q_N^T is a two-dimensional space-time continuum ($N=2$), whose dimensions correspond to the physical size of the CA lattice. We assume that both D and h are piecewise continuous, non-negative functions; m and q are positive real numbers; k is a non-negative constant matrix defined on Q_N^T and δ_0 is the Dirac delta function that represents the source at time $t=0$. The evolution of source in time and in space is given by $f(\vec{x},t)$. Eq. (1) has a non-negative solution that corresponds to the physical and biological properties of systems and processes modeled in this work [44].

Eq. (1) was studied theoretically in [45]. The authors first considered the case when $D \equiv 1$, $h \equiv 0$ and $m > (N-2)/2$ and defined a corresponding solution $B_k(x,t)$ for any $k > 0$ (here k corresponds to the initial condition of (1)):

$$B_k(x,t) = t^{-l}\left(C_k - \frac{(m-1)l|x|^2}{2mNt^{2l/N}}\right)^{1/(m-1)} \tag{2}$$

where

$$l = \frac{N}{N(m-1)+2}, \quad C_k = a(m,N)k^{2(m-1)l/N},$$

and $a(m,N)$ is a free parameter. Note that $B_k(x,t)$ is also known as the "Barenblatt solution" [44].

Since B_k is a supersolution for problem (1), a sufficient condition for existence (and uniqueness) of u_k is

$$\iint_{Q^T} B_k(x,t)h(t)\,dx\,dt < \infty. \tag{3}$$

By change of variable $y = t^{l/N}x$, this condition becomes independent of $k > 0$. The authors in [45] have proved that *if*

$$\int_0^1 h(t)t^{l-lq}\,dt < \infty, \tag{4}$$

when $m > 1$, $q > 0$, *then* the problem (1) admits a unique positive solution $u = u_k$.

4.2. Carcinogen penetration

The carcinogens mixed with the solute, in the form of biofluid, penetrate through the bladder wall into the deep layers of urothelium. If the carcinogen concentration inside the basal cells passes certain threshold, it triggers the chain of mutations, leading potentially to the cells with the cancerous phenotype. Below we summarize the number of assumptions we made to model the penetration process (in accordance with [46]):

1. The carcinogen is accumulating on the bladder wall.
2. The carcinogen penetrates slowly through the layers of urothelium and its concentration reaches mutation threshold level in the years-long span.
3. Cell loss (both apoptosis and necrosis) leads to the "empty space" in the lattice with no carcinogen [47].

In this work we generalize the model of carcinogen penetration suggested in [3]. Carcinogen penetration is modeled within the same mathematical framework as oxygen diffusion (Eq. (1)) and defined on the same physical domain. However, diffusion and absorption coefficients for carcinogen penetration are different and correspond to the values obtained from the toxicology studies as detailed in Table 2. The carcinogen concentration is measured as [amount of solute per cell volume]=[mol/L]. The speed of carcinogen penetration is much slower than the speed of oxygen diffusion, as reflected in the corresponding coefficients in Table 2. It has been proven experimentally (see, for instance, [48]) that majority of carcinogens are absorbed through simple passive diffusion. The degrees of proportionality $m-1$ and $q-1$ of diffusion and absorption coefficients are adjusted experimentally as well. The concentration of carcinogens on the bladder wall is random throughout the simulation and it is updated at the beginning of each CA time-step.

5. Angiogenesis

The tumor cannot grow beyond the certain size (usually, 1–2 mm^3) by exploiting resources of the urothelium [49]. Its further growth requires additional oxygen and nutrients provided by the neovascular network developing towards the tumor. These new blood vessels have a very chaotic structure and have a higher permeability compared to the regular vascular system. The new blood vessels are more leaky and carry with them less oxygen and nutrients than the regular blood vessels. However, they provide surrounding normal and cancer cells with easier access to oxygen and nutrients than the blood vessels lying in the lamina propria.

Responding to the insufficient oxygen supply the cancer cells overexpress and activate HIF (specifically, HIF-1α). The latter activates expression of vascular endothelial growth factor (VEGF), the secreted protein capable of signaling towards the lamina propria. VEGF is one of the key angiogenic factors that stimulates formation of the new blood vessels and tumor growth [50]. Elevated levels of VEGF expression were detected in the urine samples from the BC patients and correlated with the disease recurrence and progression [51]. In agreement with this study, a high level of the VEGF expression that was present in tumors and in serum samples from patients with BC, also predicted a poorer prognosis and an increased frequency of disease recurrence [43]. Interestingly, simultaneously to promoting angiogenesis via VEGF, HIF-1α promotes invasion of malignant cells through tissues via other mechanisms. Therefore, the increased angiogenesis might associate with both increased rate of tumor growth and promotion of invasion processes, two main markers of a disease progression.

Our approach to the simulation of angiogenesis could be described as follows:

1. The mutated cell has obtained cancer phenotype, but it does not have sufficient amount of nutrients and oxygen necessary for proliferation (oxygen level below $L3$).
2. The cell sends the VEGF signal to the vascular network located in the lamina propria.
3. As soon as the VEGF signal reaches the closest cell in lamina propria; the blood vessels start to branch away from this cell and work as a source of oxygen and nutrients for all surrounding cells with increased diffusion coefficient due to its high permeability [49].
4. On each CA time step, the blood vessels grow towards the cancer cells by capturing empty space or replacing (killing) basal and ordinary cells located on their path.
   The tip cells of the angiogenic sprouts secrete enzymes such as matrix metalloproteinases (i.e. MMP-9) that lead to the degradation of the extra-cellular matrix (ECM) and eventual death of the cells lying on the pass between the newly formed blood vessels and the developing tumor [52,53]. One should also notice that MMPs help degrade the proteins that keep the vessel walls solid [54].
5. Other cancer cells with insufficient level of oxygen send the VEGF signal that could reach either lamina propria or newly formed vessels and start new sprouts, effectively building the angiogenesis tree.

The structure of the neovascular network depends on the type of BC [55]. The new vessels are confined within the polyp when it grows into the bladder lumen and they eventually kill the tumor cells.

As result of the angiogenic activity the urothelium looses its elasticity resulting in blood leaking into the bladder that is usually detected through the discovery of blood traces in the urine sample.

6. Numerical simulations

6.1. Settings

In order to simulate BC growth on computer we make the number of assumptions in addition to ones discussed in the previous sections:

- We assume that an ordered sequence of four specific mutations is sufficient for basal cell to obtain a BC phenotype [18–28].
- In our experiments, angiogenesis is regulated by HIF [51]. We simulate the effect of hypoxia on ordinary, basal and cancer cells by setting the corresponding oxygen level thresholds (see Table 1).
- We ignore the geometry of the cell.

Table 1 is used to connect between the CA and the models of continuous processes as shown in Fig. 8. On each CA iteration, the actual values of oxygen level and carcinogen concentration are checked against the threshold values for each cell. The changes in the cell state vector (e.g., cell status and mutation counter) are introduced then. The values in Table 1 are given as the references. They had been estimated for the US Environmental Protection Agency (USEPA) using the methodology detailed in [56].

In the simulation of continuous processes, we consider an xy-plane, such that the horizontal x-axis goes along and the vertical y-axis goes down through the layers of urothelium. We assume that the carcinogens penetrate from top to bottom of

Table 1
The threshold values used in the CA model.

Name of the threshold	Value (mol/L)	References
Oxygen concentration level $L1$ (above $L1$: sufficient for basal cell proliferation)	4.5×10^{-4}	[57]
$L2$ (above $L2$: sufficient for life for ordinary and basal cells, but insufficient for basal cell proliferation; below $L2$: ordinary and basal cell apoptosis under hypoxia)	1.5×10^{-4}	Estimated 1/3 of $L1$ following [34]
$L3$ (above $L3$: sufficient for cancer cell proliferation)	4.5×10^{-5}	[29]
$L4$ (above $L4$: sufficient for cancer cell life, but insufficient for its proliferation; below $L4$: cancer cell enters the sleeping state for 1 year and dies after that)	1.5×10^{-5}	[29]
Carcinogen concentration level $C1$ (mutation threshold in the basal cells and necrosis threshold in the ordinary cells)	1.5×10^{-4}	[58]

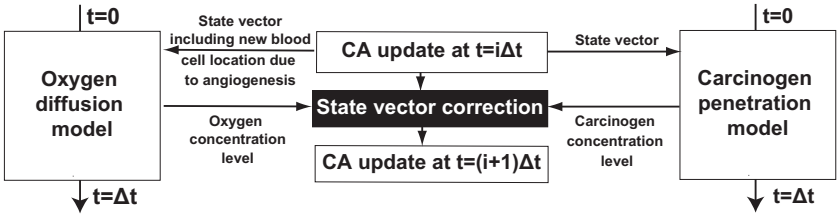

Fig. 8. Combination of the discrete CA model of urothelial cell dynamics with the continuous models of carcinogen penetration and oxygen diffusion. Δt is a period of time between updates of the cell states in accordance with the CA rules. i is the number of iteration (update). The data transferred between the models is detailed in Section 6 dedicated to numerical experiments.

urothelium; the oxygen diffusion starts from the bottom of urothelium, but could eventually start and go in any direction following development of the neovascular network due to the angiogenesis. In the BC scenarios discussed in this work, the tumor grows towards the bladder lumen and yields a polyp or remains within the urothelium forming a CIS.

The diffusion coefficients for both carcinogen penetration and oxygen diffusion models (summarized in the Table 2) are piecewise constant, and their values depend on the cell type. Newly formed blood vessels have very high permeability [49], as result they do not curry as much oxygen and nutrients as regular vessels. Using the available data (see also [59]) we estimate their oxygen concentration is half that of the oxygen concentration in regular blood vessels.

The absorption (uptake) coefficients are equal to $0.1\ s^{-1}$ for oxygen diffusion model [60] and to $1\ s^{-1}$ for carcinogen penetration model [61].

There is no clear rule for choosing parameters m and q for each model. So we consider $m = q = 2$ for carcinogen penetration, which brings it in line with the classical porous medium equation. Oxygen diffusion is modeled with $m=2$ and $q=3$. In practice, these two processes have a different time scale: carcinogen penetration is a very slow process, while oxygen diffusion is supposed to be much faster [62].

In our numerical experiments, we consider a small part of the urothelium – a rectangular slice that corresponds to ~ 2000 cells (roughly 2% of the urothelium cross-section). In order to avoid numerical artifacts leading to increased carcinogen concentration and fast tumor growth near the boundaries we add the so-called *buffer layers* from both sides of the computational domain.

In normal urothelium, the carcinogens are stopped by the basement membrane. The effect of carcinogen penetration into the fat and muscle layers and further deep into the surrounding tissues is related to the MMPs secreted by the cancer cells following a specific chain of mutations modeled in [6].

We consider the oxygen concentration within the regular blood vessels to be equal to 5.175×10^{-3} mol/L at the beginning of each CA time-step [63]. The carcinogen on the bladder wall is uniformly distributed and its maximum is estimated as 3×10^{-6} mol/L, which corresponds to the average cotinine concentration in the urine of the active smokers [64]. Cotinine, a nicotine metabolite, is a biomarker of tobacco, nicotine, and carcinogen exposure.

Eq. (1) is solved numerically by the 4th order finite difference algorithm for integration in space and the 4th order Runge–Kutta scheme for advancing in time [65]. The algorithm is able to handle a situation when the carcinogen concentration within the solute changes rapidly and sharply. We also did a perturbation analysis to confirm that small changes in parameter values do not lead to significant changes in the outcome of our numerical simulations. The temporal resolution of continuous models is chosen to ensure

Table 2
The diffusion coefficients for various cell types used in the simulation of continuous processes. The references are (a) Androjna et al., Tissue Eng. A 14 (4) (2008) 559–569, (b) J. Pfeuffer et al., J. Cereb. Blood Flow Metabol. 20 (4) (2000) 736–746, (c) T. B. Bentley et al., Am. J. Physiol. 264 (1993) H1825, (d) R. Venkatasubramanian, et al., J. Theor. Biol. 242 (2) (2006) 440–453, (e) E. Selard et al., Spine 28 (2003) 1945–1953, (f) K.L. Weind, et al., Am. J. Physiol. 281 (2001) H2604, (g) O. Boubriak, J.P.G. Urban, J. Bone Joint Surg. 84 (I) (2002): 93d, (h) B.M. Fu, et al., J. Biomech. Eng. 127 (2) (2005) 270–278.

Cell type	Oxygen $(cm^2/s) \times 10^{-5}$	Diffusion reference	Carcinogen $(cm^2/s) \times 10^{-5}$	Penetration reference
Empty space in lattice	4.6	(a)	1.35	(b)
Bladder lumen	0.6	Based on (a)	0.4	(b)
Muscle and fat	2.1	(c)	0.01	*
Normal	1.82	(d)	0.486	(e)
Cancer	1.29	(f)	1.0	**
Blood cells (in lamina propria)	1.06	(f)	0.176	(g)
New blood cells (angiogenesis)	4.25	(f,h)	0.7	Based on (g)

* Estimation based on H. Sorbye et al., Dig. Dis. Sci. 40 (12) (1995) 2509–2515.
** Estimation based on J.P. Berry et al., Ann. Clin. Lab. Sci. 15 (2) (1985) 109–120.

the stability of numerical solution. In physical terms it is equal to ~4 min (duration of one CA iteration is 24 h). A very small artificial viscosity is added through the fourth order spatial derivative (with coefficient of order 10^{-9}).

In the numerical experiments presented in this work, both the cell dynamics and the continuous processes are modeled using the same spatial resolution ($\Delta x = \Delta y = h$ and $h^2 =$ [average cell area]). However, in general, each unit cell of CA could be represented by the multiple cells on the grid used for the discretization of the continuous processes. In such a case, carcinogen and oxygen levels transferred to the CA model are integrated over the area of the corresponding urothelial cell.

The time span of both continuous models is corresponding to the single time-step of the CA, which is equal to one day in our experiments. As shown in Fig. 8, the continuous models update the cell state vector in CA model and obtain the initial conditions, the values of coefficients and the values of carcinogen and oxygen concentration levels from the previous time step.

In the next sections we discuss numerical simulations representing two common scenarios of BC progression: bladder polyp and carcinoma in situ (CIS).

6.2. Bladder polyp

Bladder polyps are the most common form of the urinary bladder carcinoma. Their main macroscopic features are single or multiple exophytic papillary masses [66]. In our simulations, we follow the process of polyp formation starting from the clones of mutated cells within the urothelium. Growth of polyps is always supported by the angiogenesis [16] and it is also reflected in our experiments. As we have already stated in Section 2, BC development and progression is a long multi-year process. In the bladder polyp scenario presented in this work we make the *85 months* snapshots of cell status (Fig. 9(a)) and carcinogen penetration and oxygen diffusion (Fig. 10(a) and (b) respectively). By that time we have two full grown polyps within the bladder lumen and the number of smaller polyps of various sizes. The similar scenarios are often observed during bladder polyp removal surgery.

The neovascular network (shown in red in Fig. 9(a)) grows through the urothelium toward the polyp and eventually ruins the layered structure of urothelium and changes its physical characteristics. Our simulation reflects an important morphological feature of angiogenic behavior in the bladder polyp form of BC: the blood vessels grow within the polyp [55]. One more observation corresponds to the particular BC scenario run in the simulation: most basal cells have already obtained the cancer phenotype by the snapshot time. It means that the surgical removal of polyp and its neovascular network will not eradicate BC. With high probability, the urothelial cells damaged during the surgery and the post-surgery treatment will be replaced by the cancerous cells. New polyps will continue to grow, and the BC remission is the expected follow-up scenario.

The carcinogen concentration in Fig. 10(a) is highest for umbrella cells. This reflects the role of umbrella cells within the urothelium: to slowdown the penetration process and prevent from the carcinogens reaching the basal cells. One can observe from Fig. 10(a) that the carcinogens are also absorbed by the polyps.

The oxygen level in Fig. 10(b) mimics the geometry of polyps and corresponds to their morphology. The new blood vessels formed as the result of the angiogenic activity provide the cancerous cells with oxygen and nutrients sufficient for the polyp growth.

6.3. Carcinoma in situ (CIS)

The CIS is caused by the different chain of mutations than the polyp [18]. In Fig. 11, we show the CIS modeled using our approach (a) and the cross-section of CIS from the cystoscopy (b). On the *in vivo* images the CIS is marked by brown color and one can see that it spreads within the urothelium barely leaving the umbrella cells. According to [66], the major macroscopic properties of the CIS are granular or cobblestone appearance (as seen in Fig. 11(b)) and multifocality.

One can also see that our simulation has also captured a major morphological characteristics of CIS: its “mushroom-like shape”.

7. Discussion and future work

In this work, we have presented an *in silico* model of urinary bladder carcinoma development and growth. In our simulations, we demonstrated the cell dynamics corresponding to the development of low-grade BC in the form of bladder polyps and CIS. The main purpose of our numerical experiments was to study the

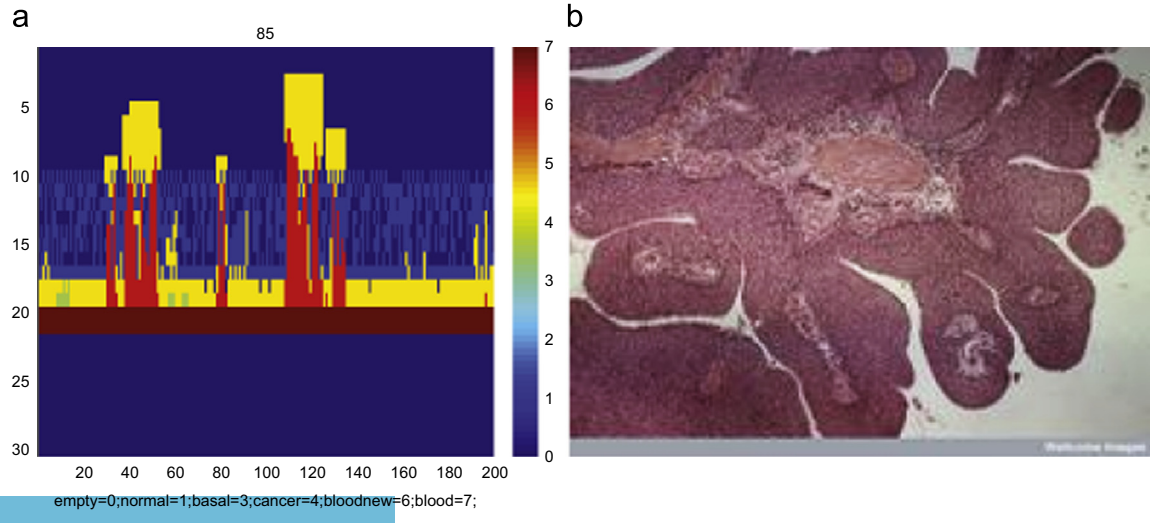

Fig. 9. Snapshot from the simulation of polyp growing into the bladder lumen (a) and image of polyps from the cystoscopy provided as reference (⟨http://healthtap.com⟩) (b). (For interpretation of the references to color in this figure caption, the reader is referred to the web version of this paper.)

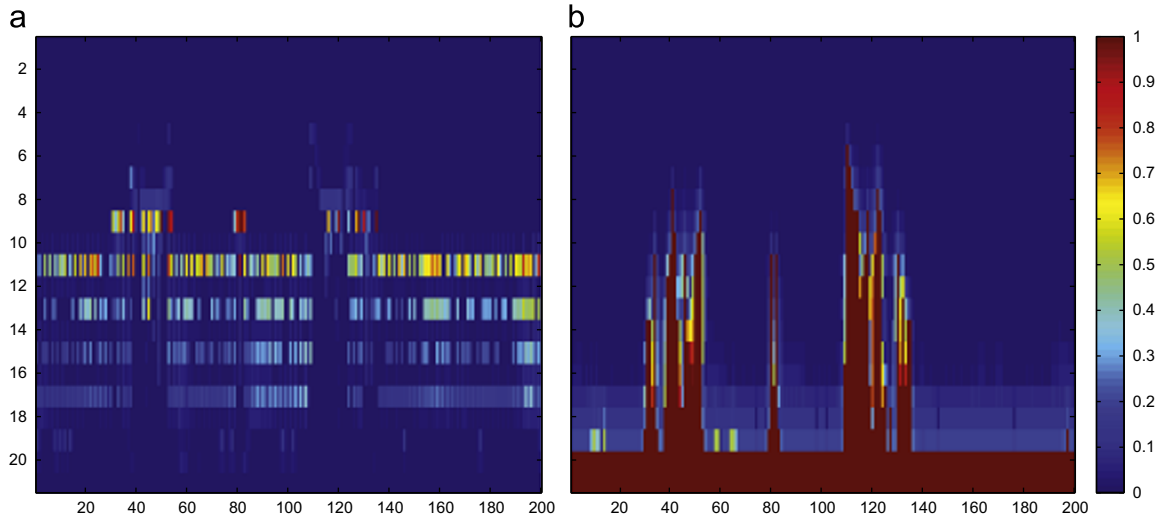

Fig. 10. Concentration of carcinogens within the urothelium (a) and oxygen level (b) corresponding to the simulation of bladder polyp in Fig. 9(a).

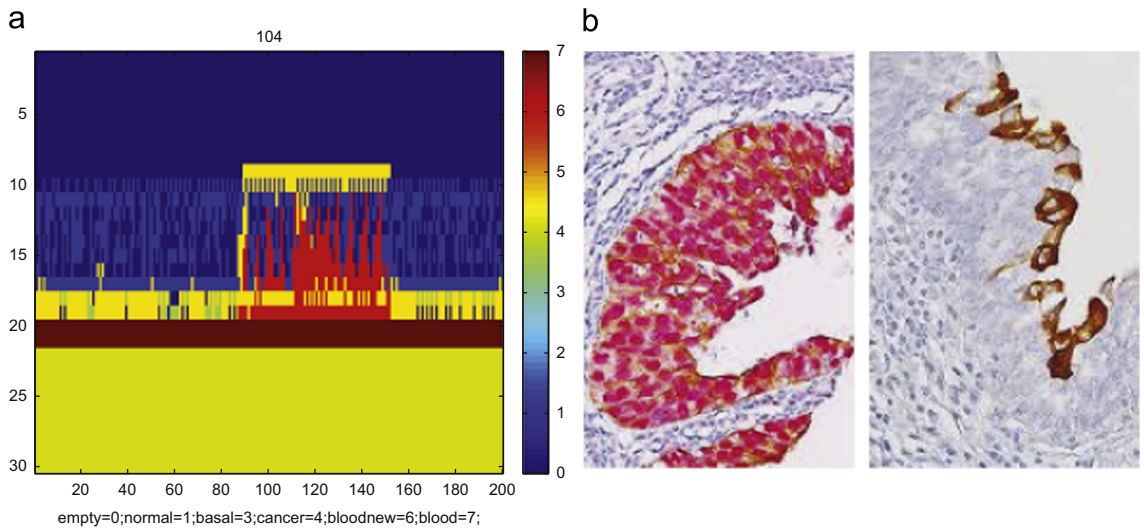

Fig. 11. CIS: numerical simulation (a) and cystoscopy image from ⟨http://pathologyoutlines.com⟩ (b). (For interpretation of the references to color in this figure caption, the reader is referred to the web version of this paper.)

effects of carcinogen penetration and hypoxia and to understand the role the angiogenesis is playing in the BC progression.

In our previous work [3,6], we introduced a framework that combines discrete and continuous models to describe quantitatively the BC initiation. However, the current model represents a major revision of our approach and its significant extension. It allows us to simulate bladder carcinogenesis from the initial mutations to the full-size tumor. The nonlinear submodel of oxygen diffusion and the CA-based submodel of angiogenesis, presented in this paper, could be used for modeling and simulation of various cancers, originating in epithelial cells.

One of the major challenges in cancer urology is to provide a prognosis of tumor development for a patients based on the information collected from the cystoscopy and the initial treatment. If such a prognosis could be done early in the course of treatment, those with a high likelihood of BC recurrence or progression could be treated more aggressively. A histological examination is used to predict the probability of recurrence and the progression of low-grade urinary bladder carcinoma. From the analysis of the cell structure, the pathologist determines the stage, grade, and multiplicity of tumor. However, the accuracy of such an examination depends on the pathologist's experience.

The current consensus is that these tumors evolve down one of two major genetic pathways. The first is associated with low-grade papillary and non-invasive cancers that infrequently progress to invasive BC. The other is typified by *in situ* or higher grade superficial tumors that frequently recur and progress to higher grade and muscle invasive disease [67]. Given individual patient data and genetic analysis of the biopsy, our model will be able to comprehend the diagnostics process by analyzing various scenarios of tumor behavior and make both qualitative and good first-order quantitative predictions of tumor development.

Bladder tumors have diverse morphology [14] and this situation significantly complicates their diagnosis. In many cases, BC may contain variable proportions of different histologic patterns. The clinical outcome of some variants differs from that of typical urothelial carcinoma and may call for different therapeutic approaches. Pathologists should also be aware of the incidence and histologic appearances of secondary neoplasms of the urinary

bladder, with emphasis on the points of distinction from primary tumors and their histologic variants [68]. Comparison of the computer-predicted and actually observed tumor patterns may help clinicians with better understanding of tumor histology and planning of treatment strategy.

Conflict of interest

None declared.

Acknowledgments

The authors want to thank to Prof. Helen Byrne from the Mathematics Institute of Oxford University for fruitful discussions that led to the development of BC modeling framework presented in this paper. We also acknowledge the work done by the anonymous reviewers and the Editor whose comments and suggestions helped us to raise the quality of the paper.

References

[1] A. Jemal, et al., Global cancer statistics, CA: A Cancer J. Clin. 61 (2011) 69–90.
[2] M. Burger, et al., Epidemiology and risk factors of urothelial bladder cancer, Eur. Urol. 63 (2) (2013) 234–241.
[3] E. Kashdan, S. Bunimovich-Mendrazitsky, Multi-scale model of bladder cancer development, Discret. Contin. Dyn. Syst. Suppl. (2011) 803–812.
[4] K.R. Swanson, E.C. Alvord Jr., J.D. Murray, A quantitative model for differential motility of gliomas in grey and white matter, Cell Prolif. 33 (2000) 317–329.
[5] H.M. Byrne, et al., Modelling the response of vascular tumours to chemotherapy: a multiscale approach, Math. Models Methods Appl. Sci. 16 (2006) 1219–1241.
[6] E. Kashdan, S. Bunimovich-Mendrazitsky, Hybrid discrete-continuous model of invasive bladder cancer, Math. Biosci. Eng. 10 (2013) 729–742.
[7] V. Kumar, A.K. Abbas, N. Fausto, Robbins and Cotran Pathological Basis of Disease, 7th ed. Elsevier, Philadelphia, 2005 (Chapter 21).
[8] D. Shier, J. Butler, R. Lewis, Hole's Human Anatomy and Physiology, 13th ed., McGraw-Hill, New York, 2012.
[9] P.J. Woodroffe, et al., Modelling cell signalling and differentiation in the urothelium, Bull. Math. Biol. 67 (2005) 369–389.
[10] P.L. Ho, A. Kurtova, K.S. Chan, Normal and neoplastic urothelial stem cells: getting to the root of the problem, Nat. Rev. Urol. 9 (10) (2012) 583–594.
[11] K. Shin, et al., Cellular origin of bladder neoplasia and tissue dynamics of its progression to invasive carcinoma, Nat. Cell Biol. 16 (5) (2014) 469–478.
[12] J. Adamowicz, et al., The relationship of cancer stem cells in urological cancers, Cent. Eur. J. Urol. 66 (3) (2013) 273–280.
[13] A. Staack, et al., Molecular, cellular and developmental biology of urothelium as a basis of bladder regeneration, Differentiation 73 (2005) 121–133.
[14] J.N. Eble, R.H. Young, Carcinoma of the urinary bladder: a review of its diverse morphology, Semin. Diagn. Pathol. 14 (2) (1997) 98–108.
[15] W. Hassen, M.J. Droller, Current concepts in assessment and treatment of bladder cancer, Curr. Opin. Urol. 10 (2000) 291–299.
[16] B. George, R.H. Datar, R.J. Cote, Molecular biology of bladder cancer: cell cycle alterations, in: S.P. Lerner, M.P. Schoenberg, C.N. Sternberg (Eds.), Textbook of Bladder Cancer, Taylor and Francis, Boca Raton, Florida, 2006, pp. 107–122.
[17] M.A. Knowles, Molecular subtypes of bladder cancer: Jekyll and Hyde or chalk and cheese? Review, Carcinogenesis 27 (3) (2006) 361–373.
[18] S. Brandau, A. Böhle, Bladder cancer. I. Molecular and genetic basis of carcinogenesis, Eur. Urol. 39 (2001) 491–497.
[19] J.H. Guth, The mechanism of asbestos-induced carcinogenesis: calcium and plasma membrane integrity, in: Proceedings of the 59th Meeting of Virginia Academy of Sciences, Norfolk, VA, 1981.
[20] D. Theodorescu, Molecular pathogenesis of urothelial bladder cancer, Histol. Histopathol. 18 (2003) 259–274.
[21] E.J. Tokar, L. Benbrahim-Tallaa, M.O. Waalkes, Metal ions in human cancer development, Met. Ions Life Sci. 8 (2011) 375–401.
[22] K.E. Eblin, T.G. Bredfeldt, A.J. Gandolfi, Immortalized human urothelial cells as a model of arsenic-induced bladder cancer, Toxicology 248 (2–3) (2008) 67–76.
[23] M. Yang, A current global view of environmental and occupational cancers, J. Environ. Sci. Health C 29 (3) (2011) 223–249.
[24] D. Beyersmann, Effects of carcinogenic metals on gene expression, Toxicol. Lett. 127 (1-3) (2002) 63–68.
[25] S. Somji, et al., Comparison of expression patterns of keratin 6, 7, 16, 17, and 19 within multiple independent isolates of As(+3)- and Cd(+2)-induced bladder cancer, Cell Biol. Toxicol. 27 (6) (2011) 381–396.
[26] R.L. Carpenter, B.H. Jiang, Roles of EGFR, PI3K, AKT, and mTOR in heavy metal-induced cancer, Curr. Cancer Drug Targets 13 (3) (2013) 252–266.
[27] M. Feki-Tounsi, et al., Trace metal quantification in bladder biopsies from tumoral lesions of Tunisian cancer and controls subjects, Environ. Sci. Pollut. Res. Int. 21 (19) (2014) 11433–11438.
[28] J.B. Cazier, et al., Whole-genome sequencing of bladder cancers reveals somatic CDKN1A mutations and clinicopathological associations with mutation burden, Nat. Commun. 5 (2014) 3756.
[29] T. Alarcon, H.M. Byrne, P.K. Maini, A cellular automaton model for tumour growth in inhomogeneous environment, J. Theor. Biol. 225 (2003) 257–274.
[30] Transitional Epithelium of the Urinary Bladder. ⟨http://en.wikipedia.org/wiki/Urothelium⟩. Image available for use under CCA license.
[31] A.M. Klein, B.D. Simons, Universal patterns of stem cell fate in cycling adult tissues, Development 138 (2011) 3103–3111.
[32] N.T. Gaisa, et al., The human urothelium consists of multiple clonal units, each maintained by a stem cell, J. Pathol. 225 (2011) 163–171.
[33] K. Shin, et al., Hedgehog/Wnt feedback supports regenerative proliferation of epithelial stem cells in bladder, Nature 472 (7341) (2011) 110–114.
[34] B. Alberts, et al., Molecular Biology of the Cell, Garland Science, New York, 5th ed., 2008 (Chapter 17).
[35] S. Durinck, et al., Temporal dissection of tumorigenesis in primary cancers, Cancer Discov. 1 (2011) 137–143.
[36] J. Pellettieri, A. Sanchez Alvarado, Cell turnover and adult tissue homeostasis: from humans to planarians, Annu. Rev. Genet. 41 (2007) 83–105.
[37] J. Southgate, et al., Urothelial tissue regulation, in: S. Baskin, S.W. Hayward (Eds.), Advances in Bladder Research, vol. 462, 1999, pp. 19–30.
[38] K.W. Kinzler, B. Vogelstein, Life (and death) in a malignant tumour, Nature 379 (1996) 19–20.
[39] T.G. Fellous, S.A. McDonald, J. Burkert, A methodological approach to tracing cell lineage in human epithelial tissues, Stem Cells 27 (2009) 1410–1420.
[40] S.M. Wnek, et al., Persistence of DNA damage following exposure of human bladder cells to chronic monomethylarsonous acid, Toxicol. Appl. Pharmacol. 241 (2009) 202–209.
[41] J.A. Royds, et al., Response of tumour cells to hypoxia: role of p53 and NFkB, J. Clin. Pathol.: Mol. Pathol. 51 (1998) 55–61.
[42] G.N. Naumov, et al., A model of human tumor dormancy: an angiogenic switch from the nonangiogenic phenotype, J. Natl. Cancer Inst. 98 (5) (2006) 316–325.
[43] O. Sagol, K. Yorukoglu, B. Sis, Does angiogenesis predict recurrence in superficial transitional cellcarcinoma of the bladder? Urology 57 (2001) 895–899.
[44] J.L. Vasquez, Porous Medium Equation. Mathematical Theory, Oxford University Press, Oxford, 2007.
[45] A. Shishkov, L. Veron, The balance between diffusion and absorption in semilinear parabolic equations, Rend. Lincei—Mat. Appl. 18 (2007) 59–96.
[46] G.P. Hemstreet III, E.M. Messing, Early detection for bladder cancer, in: S.P. Lerner, M.P. Schoenberg, C.N. Sternberg (Eds.), Textbook of Bladder Cancer, Taylor and Francis, Boca Raton, Florida, 2006, pp. 257–266.
[47] R.W. Vandivier, P.M. Henson, J.S. Douglas, Burying the dead*: the impact of failed apoptotic cellremoval (efferocytosis) on chronic inflammatory lung disease, CHEST 129 (6) (2006) 1673–1682.
[48] U.S. EPA. Guidelines for Exposure Assessment. U.S. Environmental Protection Agency, Risk Assessment Forum, Washington, DC, EPA/600/Z-92/001, 1992.
[49] J. Folkman, Tumor angiogenesis: therapeutic implications, N. Engl. J. Med. 285 (1971) 1182–1186.
[50] D.M. Aebersold, P. Burri, K.T. Beer, Expression of hypoxia-inducible factor-1α: a novel predictive and prognostic parameter in the radiotherapy of oropharyngeal cancer, Cancer Res. 61 (2001) 2911–2916.
[51] A. Jones, C. Fujiyama, C. Blanche, Relation of vascular endothelial growth factor production to expression and regulation of hypoxia-inducible factor $1-\alpha$ and hypoxia-inducible factor $2-\alpha$ in human bladder tumors and cell lines, Clin. Cancer Res. 7 (2001) 1263–1272.
[52] S. Turner, J.A. Sherratt, Intercellular adhesion and cancer invasion: a discrete simulation using the extended potts model, J. Theor. Biol. 216 (1) (2002) 85–100.
[53] T. Bugge, et al., Growth and dissemination of Lewis lung carcinoma in plasminogen-deficient mice, Blood 90 (11) (1997) 4522–4531.
[54] B.M. Prior, H.T. Yang, R.L. Terjung, What makes vessels grow with exercise training? J. Appl. Physiol. 97 (3) (2004) 1119–1128.
[55] F. Hillen, A.W. Griffioen, Tumour vascularization: sprouting angiogenesis and beyond, Cancer Metastasis Rev. 26 (3–4) (2007) 489–502.
[56] US EPA, Risk Assessment Guidance for Superfund (RAGS) Part A ⟨http://www.epa.gov/oswer/riskassessment/ragsa⟩ (Chapter 7).
[57] A.A. Patel, et al., A cellular automaton model of early tumor growth and invasion, J Theor. Biol. 213 (3) (2001) 315–331.
[58] H.G. Neumann, Risk assessment of chemical carcinogens and thresholds, Crit. Rev. Toxicol. 39 (6) (2009) 449–461.
[59] R.K. Jain, Transport of molecules in the tumor interstitium: a review, Cancer Res. 47 (1987) 3039–3051.
[60] J.J. Casciari, S.V. Sotirchos, R.M. Sutherland, Variations in tumor cell growth rates and metabolism with oxygen concentration, glucose concentration, and extracellular pH, J. Cell. Physiol. 151 (2) (1992) 386–394.
[61] K.A. Rejniak, et al., The role of tumor tissue architecture in treatment penetration and efficacy: an integrative study, Front. Oncol. 3 (2013) 1–13.
[62] G.A. Truskey, F. Yuan, D.F. Katz, Transport Phenomena in Biological Systems, 2nd ed., Prentice Hall, Upper Saddle River, New Jersey, 2009.
[63] R. Valabérgue, et al., Relation between cerebral blood flow and metabolism explained by a model of oxygen exchange, J. Cereb. Blood Flow Metabol. 23 (2003) 536–545.

[64] A. Florescu, et al., Methods for quantification of exposure to cigarette smoking and environmental tobacco smoke: focus on developmental toxicology, Ther. Drug Monitor. 31 (1) (2009) 14–30.
[65] E. Kashdan, ERWIN—High-Order Accurate Parallel Solver for Multidimensional Systems of Time-Dependent Nonlinear PDEs, Technical Report, School of Mathematical Sciences, Tel Aviv University, 2009.
[66] L. Cheng, B.J. Bock, D.G. Bostwick, Urinary Bladder, in: L. Cheng, D.G. Bostwick (Eds.), Essentials of Anatomic Pathology, Humana Press, Totowa, New Jersey, 2002 (Chapter 25).
[67] A.P. Mitra, R.H. Datar, R.J. Cote, Molecular pathways in invasive bladder cancer: new insights into mechanisms, progression, and target identification, J. Clin. Oncol. 24 (35) (2006) 5552–5564.
[68] A.W. Bates, S.I. Baithun, The significance of secondary neoplasms of the urinary and male genital tract, Virchows Arch. 440 (2002) 640–647.